

Microstructural Effects on Capacity-Rate Performance of Vanadium Oxide Cathodes in Lithium-Ion Batteries

by

Robin M. Davis

Submitted to the Department of Materials
Science and Engineering in Partial
Fulfillment of the Requirements for the
Degree of

Bachelor of Science

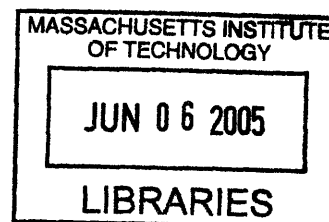
at the

Massachusetts Institute of Technology

May 2005

[June 2005]

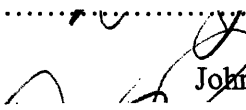
© 2005 Robin M. Davis
All rights reserved

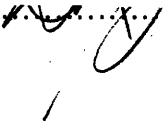


The author hereby grants to MIT permission to reproduce and to
Distribute publicly paper and electronic copies of this thesis document in whole or in
part.

Signature of Author.....

Department of Materials Science and Engineering
May 13, 2005

Certified by.....

Donald R. Sadoway
John F. Elliott Professor of Materials Chemistry
Thesis Supervisor

Accepted by.....

Donald R. Sadoway
John F. Elliott Professor of Materials Chemistry
Chairman, Undergraduate Thesis Committee

ARCHIVES

**MICROSTRUCTURAL EFFECTS ON CAPACITY RATE PERFORMANCE OF
VANADIUM OXIDE CATHODES IN LITHIUM-ION BATTERIES**

By

ROBIN M. DAVIS

**Submitted to the Department of Materials Science and Engineering
on May 13, 2005 in partial fulfillment of the
requirements for the Degree of Bachelor of Science in
Materials Science and Engineering**

ABSTRACT

Vanadium oxide thin film cathodes were analyzed to determine whether smaller average grain size and/or a narrower average grain size distribution affects the capacity-rate performance in lithium-ion batteries. Vanadium oxide thin films were prepared by sputtering onto ITO-coated glass substrates and crystallized in a refined annealing process to generate diverse microstructures. Average grain size and grain size distribution were determined in SEM analysis. No significant difference was observed in capacity rate behavior with changes in microstructure. However, it is speculated that further in situ analysis may show different relative diffusion rates into grains of differing sizes is related to different microstructures.

Thesis Supervisor: Donald R. Sadoway

Title: John F. Elliott Professor of Materials Chemistry

TABLE OF CONTENTS

| | |
|---|----|
| ABSTRACT..... | 2 |
| I. INTRODUCTION..... | 5 |
| II. LITERATURE REVIEW..... | 5 |
| III. SAMPLE PREPARATIONS..... | 9 |
| <i>X-Ray Diffraction</i> | 10 |
| <i>Scanning Electron Microscopy</i> | 14 |
| IV. ELECTROCHEMICAL ANALYSIS..... | 20 |
| <i>Capacity-Rate Performance</i> | 20 |
| <i>Atomic Force Microscopy</i> | 22 |
| <i>Galvanostatic Intermittent Titration Technique</i> | 24 |
| V. CONCLUSION..... | 27 |
| VI. ACKNOWLEDGMENTS..... | 28 |
| REFERENCES..... | 29 |

INDEX OF FIGURES

Figure 1: Schematic of Li-ion Battery.....6
Figure 2: Perspective Representation of α -vanadium Oxide Structure.....8
Figure 3: Projections of δ - and ϵ -vanadium Oxide Structure.....8

INDEX OF IMAGES

Image 1: VO131 HT1.....14
Image 2: VO131 HT2.....15
Image 3: VO131 HT3.....15
Image 4: VO131 HT4.....15
Image 5: VO132 HT1.....16
Image 6: VO132 HT2.....16
Image 7: VO132 HT3.....16
Image 8: VO132 HT4.....17
Image 9-14: In situ AFM images of VO132 HT2.....24

INDEX OF TABLES

Table 1: Sample Preparations.....10
Table 2: XRD Results.....13
Table 3: Average Grain Sizes as Determined by SEM Analysis.....19

INDEX OF GRAPHS

Graph 1: XRD Profiles of VO131 Samples.....11
Graph 2: XRD Profiles of VO132 Samples.....12
Graphs 3-10: Histograms of Sample Grain Size Distributions.....18
Graph 11: VO132 Current Rate Test Results.....21
Graph 12: GITT Results for VO132 HT2.....26

I. INTRODUCTION

Lithium-ion batteries are currently used for a variety of products, including portable electronic devices, implantable biomedical devices, and various other applications. Compared to other battery systems, lithium-ion cells can have relatively higher volumetric and gravimetric energy densities. The introduction of new products incorporating MEMS, sensors, and biomedical implants will create the need for micro energy storage. Thin-film batteries will be an attractive technology option because of their ability to generate relatively high power, thin profile, and potentially flexible form factor. In this thesis, the influence of grain size on the power capability of a vanadium oxide, thin-film cathode is examined.

Prior research has shown that it is possible to determine the diffusion coefficient of lithium in oxides via electrochemical methods^{1,2}. Diffusion behavior in sputtered vanadium oxide films with differing average grain sizes has been studied, and average grain size and grain size distribution has been related to the electrochemical behavior of the material. The rate capability was evaluated through measuring the capacity of electrochemical cells with current rate. The chemical diffusion coefficient was evaluated by the Galvanostatic Intermittent Titration Technique (GITT). Average grain size and grain size distribution of the vanadium oxide thin films were determined through X-Ray Diffraction (XRD) and Scanning Electron Microscopy (SEM).

II. LITERATURE REVIEW

The lithium battery system of interest for this research is shown schematically below.

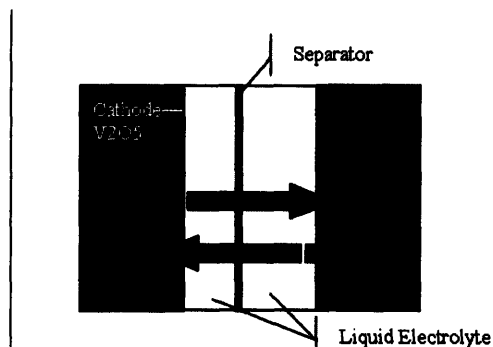


Figure 1: Schematic of Li-ion Battery

The counter and reference electrodes consist of pure lithium and the cathode is vanadium oxide (V_2O_5) sputtered onto crystalline indium tin oxide (ITO) coated glass slides. No separator is necessary, since the liquid electrolyte (1 M $LiPF_6$ in a solution of ethylene carbonate and dimethyl carbonate) isolates the individual electrodes from one another.

In cathode-material research, it is important to distinguish between the microstructural characteristics of particles and grains. Grains are adjacent crystalline regions separated by areas of misregistry of like crystal planes. These grain-boundary areas are amorphous. Particles consist of distinct crystalline regions separated by equally distinct boundaries. There is no amorphous material between particles, only void space. This research will be solely concerned with grains, as opposed to particles.

Materials with larger grains have fewer grain boundaries per unit area. Nanograins (5-50 nm diameter) can be regarded as heterogeneously disordered material composed of ordered grains and many disordered grain boundaries³. Nanograined materials have a higher disordered-to-ordered material ratio than materials with micrograins (20-100 μm diameter).

Variations in grain size can be achieved by varying the deposition conditions during sputtering and also by adjusting the time and temperature of annealing.

Furthermore,

*it is well known that the substrate surface will influence the kinetics of film growth by affecting nucleation, at least during initial nucleation of the film up to certain thickness, and the ad-layers may be affecting the subsequent growth.*⁴

Other research has shown that even distributions of grain sizes are most easily produced on crystalline substrates as opposed to amorphous substrate materials⁵.

Diffusion rates are influenced directly by material microstructure. Diffusion is usually faster along grain boundaries and free surfaces than in the bulk volume of the material. Discharge of a vanadium oxide – lithium couple is achieved by a topotactic reaction of lithium ions with the cathode⁶, consisting of insertion and diffusion of lithium ions (Li^+) into the interstitial spaces in the vanadium oxide crystal lattice. Charging of the couple is achieved by the reverse process. In theory, a material with more grain boundaries will have faster diffusion because the grain boundaries have more void space to accommodate mass transport. As the ratio of grain boundary to ordered grain within the sample decreases, the slower process of bulk diffusion within grains becomes increasingly dominant.

Other factors dictating the rate of lithium diffusion into vanadium oxide thin films include the crystal structure of bulk $\text{Li}_x\text{V}_2\text{O}_5$. As the quantity of lithium in the vanadium oxide thin films increases ($x=0 \rightarrow x=1$), the material passes through two phase transformations. All three distinct $\text{Li}_x\text{V}_2\text{O}_5$ systems encountered in this research are based on an orthorhombic crystal structure. This structure is often modeled by layers of VO_5 coordination polyhedra pyramids sharing both edges and corners (see figures 2 and

3 below). α -vanadium oxide, $\text{Li}_x\text{V}_2\text{O}_5$ where $0 < x < 0.13$, is of the space group $Pm\bar{m}n$; the ϵ -vanadium oxide, $\text{Li}_x\text{V}_2\text{O}_5$ where $0.32 < x < 0.80$ is usually of the $Cmcm$ space group, but can also be modeled using the $Pm\bar{m}n$ space group; and the δ -vanadium oxide, $\text{Li}_x\text{V}_2\text{O}_5$ where $0.88 < x < 1.00$, is also of the $Pm\bar{m}n$ space group.^{7,8}

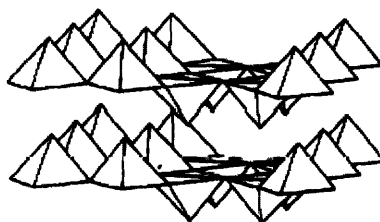


Figure 2: Perspective representation of the α - $\text{Li}_x\text{V}_2\text{O}_5$ structure assuming square-pyramidal V^{5+} coordination⁹.

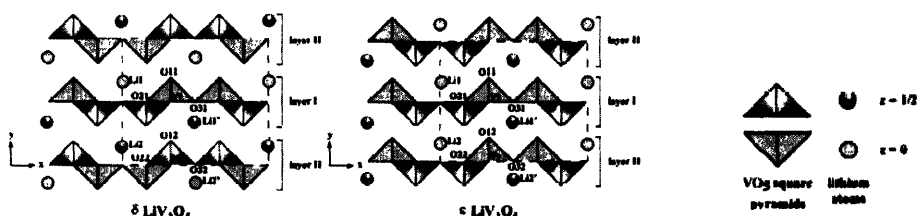


Figure 3: Projections of the δ - $\text{Li}_x\text{V}_2\text{O}_5$ and ϵ - $\text{Li}_x\text{V}_2\text{O}_5$ structures onto the (001) plane illustrating the locations for intercalated lithium.¹⁰

As lithium diffusion inserts increasing amounts of lithium into the vanadium oxide crystal, the lithium atoms are located in “distorted bicapped triangular prisms between the $[\text{V}_2\text{O}_5]$ single layers”¹¹. As more lithium atoms are intercalated into these interstitial positions, they will force an expansion between the layers of vanadium oxide coordination polyhedra. This pressure ultimately results in phase changes from α - to ϵ - to δ - $\text{Li}_x\text{V}_2\text{O}_5$ as illustrated in the images above.

The rate capability of a battery is determined by the pace at which lithium ions are able to diffuse into and out of the cathode material’s lattice. This rate of diffusion is characterized by the diffusion coefficient, which varies depending on the phase and pre-

existing lithium ion concentration in the vanadium oxide cathode. Diffusion also is typically higher along grain boundaries. As such, one would expect to see a relationship between the dominant diffusion mechanism (either grain boundary diffusion or bulk diffusion, depending on microstructure/grain size) and the rate and capacity behavior of the material. This research seeks to understand the implications of microstructure on cycling-rate performance.

III. SAMPLE PREPARATIONS

Vanadium oxide thin films were prepared by RF sputtering from a vanadium oxide target in an argon:oxygen (98:2 percent by volume) atmosphere onto indium tin oxide (ITO) coated glass slides. The target was sputtered at 300W. The substrate was unheated, although some surface heating inevitably occurs during sputtering. The sputtering rate was relatively slow at approximately 1.2 nm/min.

The sputtering process generated amorphous vanadium oxide thin films on crystalline ITO. Two separate batches of samples, VO131 and VO132, were sputtered under the same conditions to obtain multiple near-identical samples. To crystallize the vanadium oxide samples at a desired average crystalline grain size, these amorphous thin films were annealed in Lindberg/Blue tube furnaces.

Various annealing treatments were attempted and refined through experimentation to yield different average grain sizes and control the breadth of distribution of individual grain sizes about the average for each sample. The particular heat treatments for individual samples are detailed in Table 1 below. Each of the batches VO131 and VO132 was split into four sections, and each section was subjected to a unique annealing treatment.

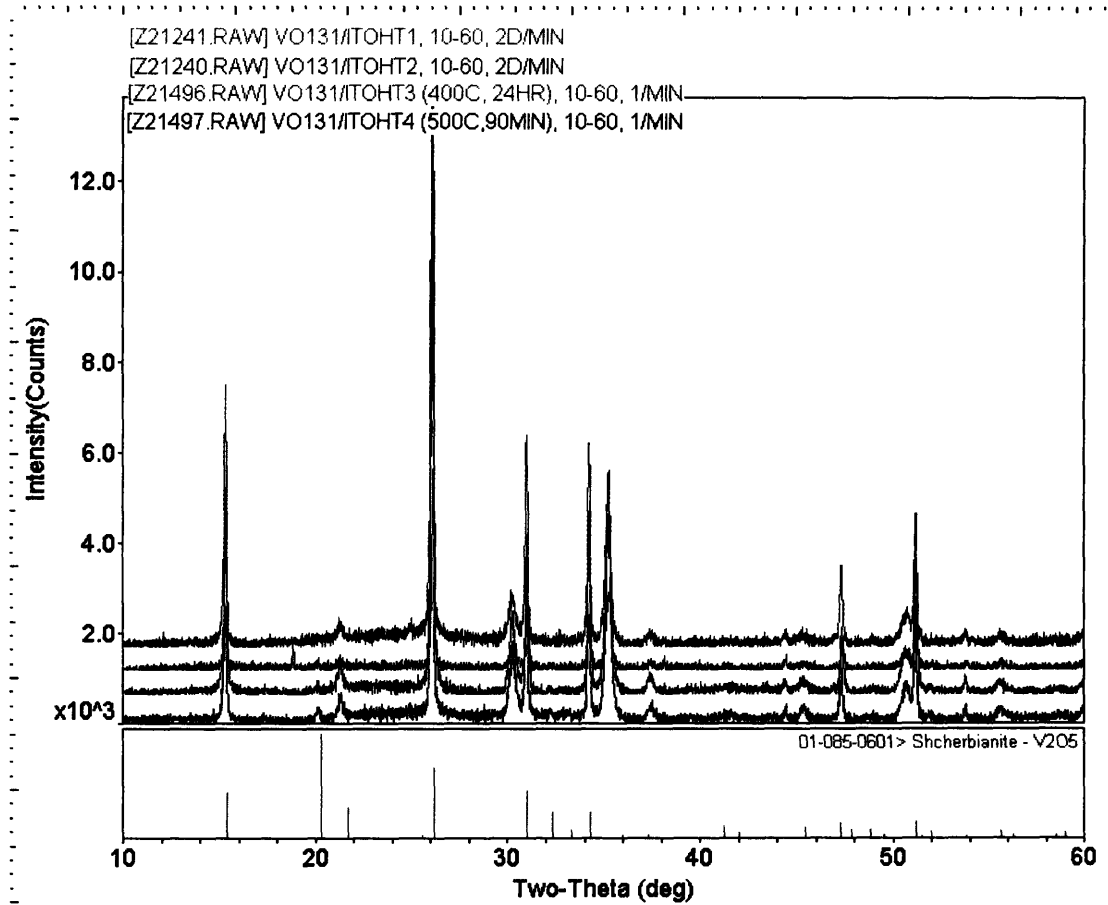
Table 1: Sample Preparations

| Sample Name | Ramp Rate (°C/min) | Hold Temperature (°C) | Hold Time |
|--------------------|--|----------------------------------|------------------|
| VO131 HT1 | 1 | 400 | 90 min |
| VO131 HT2 | N/A (sample inserted at temperature) | 400 | 90 min |
| VO131 HT3 | 70 | 400 | 24 h |
| VO131 HT4 | 70 | 500 | 90 min |
| VO132 HT1 | 0.5 | 300 | 24 h |
| VO132 HT2 | 70 | 500 | 90 min |
| VO132 HT3 | 0.5 | 500 | 90 min |
| VO132 HT4 | 1 | 400 | 90 min |

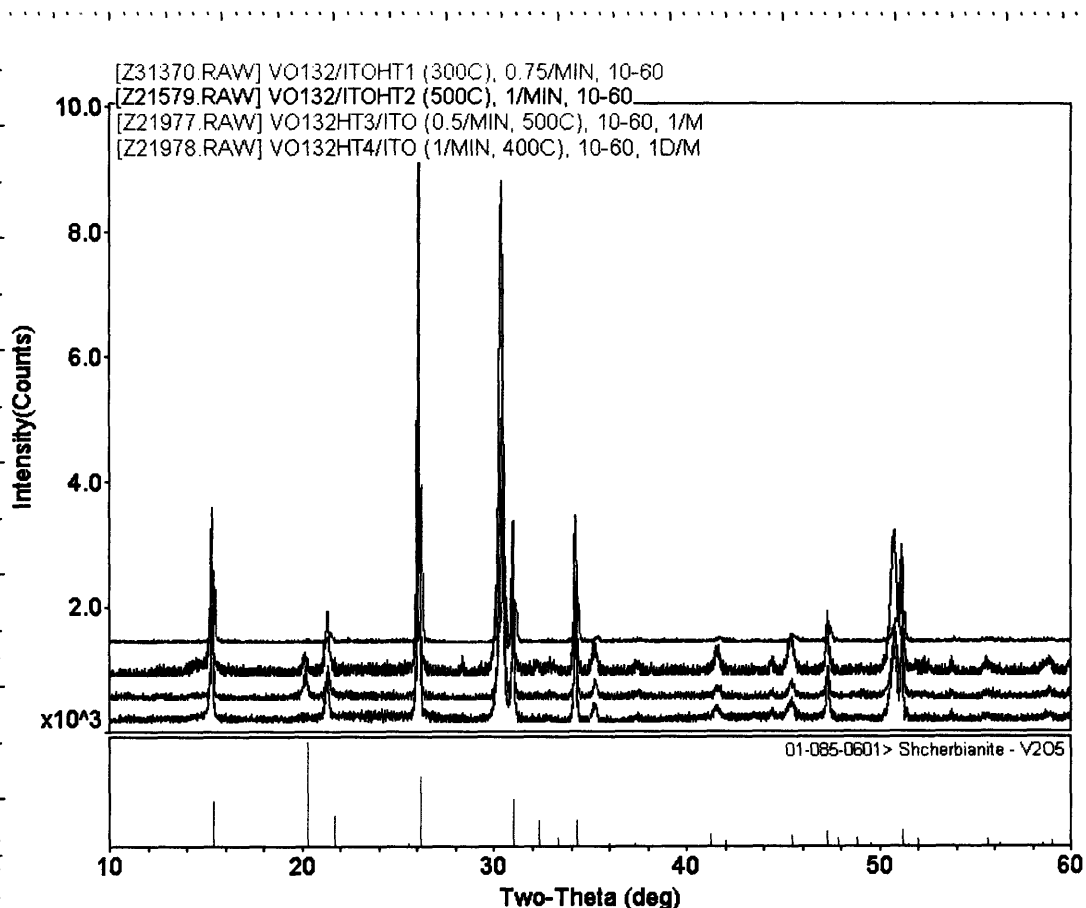
After annealing, the crystallized samples were examined with XRD to characterize their orientation, crystal structure, and lattice constants. The samples were also analyzed with SEM to determine film thickness as well as the distribution of individual grain sizes about the average grain size.

X-Ray Diffraction (XRD)

XRD measurements were conducted on a Rigaku 18 kW Rotating Anode X-Ray Generator (Copper Anode) on the crystalline samples. Scans were performed over a range of 2THETA 10-60° at a rate of 1°/min. The following graphs illustrate the XRD profiles of the samples (see graphs 1 and 2).



Graph 1: XRD Profiles of VO131 Samples



Graph 2: XRD Profiles of VO132 Samples

The lattice constant, as calculated by using peak refinement in the Jade software, remained approximately constant at 11.5 Å along the orthorhombic a-axis, 3.56 Å along the orthorhombic b-axis, and 4.40 Å along the orthorhombic c-axis. Correspondingly, the peaks from the various samples do not exhibit any noticeable shift in position.

The values of full width at half maximum (FWHM) of the characteristic vanadium oxide peaks were also calculated. The table below (Table 2) reports the average grain size as estimated by XRD measurements and the Scherrer Equation (Eqn 1). For several of the samples, the average grain size was calculated to be greater than 1000 Å and is therefore beyond the functional limits of the Scherrer Equation. For this

reason, SEM measurements of average grain size were required for all samples and must be considered more reliable estimates than values determined through XRD. The failure of the Scherrer Equation to calculate the average grain sizes for these samples is evidenced by the lack of correlation between the FWHM measurements (Table 2) and the grain sizes calculated from SEM images (Table 3).

The Scherrer Equation (for grains less than 1000 Å in size):

$$t = \frac{0.9\lambda}{B \cos\Theta} \quad (\text{Eqn. 1})$$

Where t is grain size, 0.9 is a Gaussian pre-factor, λ is the wavelength of the incident x-ray, B is FWHM, and Θ is the angle of measurement.

Table 2: XRD Results

| Sample | FWHM (weighted average across characteristic peaks) | Estimated Grain Size (Å) |
|-----------|---|--------------------------|
| VO131 HT1 | 0.154 | 664.5* |
| VO131 HT2 | 0.161 | 616.9* |
| VO131 HT3 | 0.168 | 596.0* |
| VO131 HT4 | 0.133 | 789.2* |
| VO132 HT1 | 0.105 | 751.0* |
| VO132 HT2 | 0.155 | 635.9* |
| VO132 HT3 | 0.156 | 753.0* |
| VO132 HT4 | 0.198 | 905.6* |

* = It is estimated from some of the FWHM measurements on this sample that the grain size is greater than 1000 Å and, therefore, the Scherrer Equation does not apply.

Also of note during XRD analysis was the texture of the various annealed samples. Independent of initial sputtering run (VO131 or VO132) and anneal type, all vanadium oxide thin-film samples coated on ITO exhibited a strong orientation in the <110> direction. <110> is not a known fast-diffusion direction for vanadium oxide and, as such, should have few deleterious effects on the measurement of the diffusivity of lithium ions in vanadium oxide. However, the diffusion of lithium ions is known to be

faster along $\langle 110 \rangle$ than $\langle 100 \rangle$. It is notable and unusual that there was only a very small $\langle 100 \rangle$ peak, and in some cases no $\langle 100 \rangle$ peak, in the XRD patterns of all the samples.

In light of the virtual complete absence of the $\langle 100 \rangle$ peak across samples, it was disregarded in our analysis. The insignificant changes in orientation between heat treatments also discount relative orientation as an active variable in this series of experiments.

Scanning Electron Microscopy (SEM)

To accurately determine the average grain size of samples with grains larger than 1000\AA , SEM analysis was conducted on a JEOL 6320 FEGSEM. Images were taken at a magnification of 40,000X along a cleaved edge of the thin-film samples. Grains were more easily differentiable in some samples than others, but general differences in the sizes, shapes, and distributions of grains are readily observable. Samples brought to their annealing temperature at a fast ramp rate ($70\text{ }^\circ\text{C}/\text{min}$) show a visually distinct microstructure in comparison to samples ramped to annealing temperature at a slow rate (0.5 or $1^\circ\text{C}/\text{min}$). Representative images from each of the vanadium oxide samples may be seen in Images 1-8 below.



Image 1: VO131 HT1

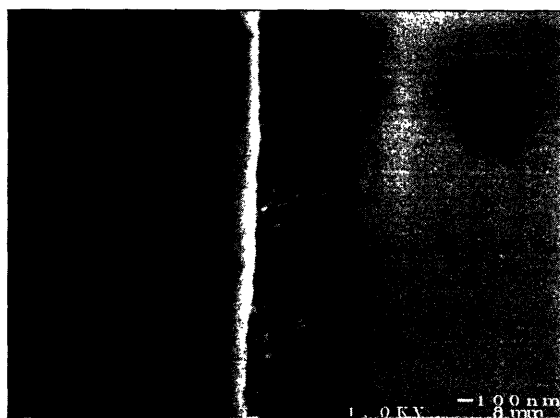


Image 2: VO131 HT2



Image 3: VO131 HT3



Image 4: VO131 HT4



Image 5: VO132 HT1



Image 6: VO132 HT2



Image 7: VO132 HT3

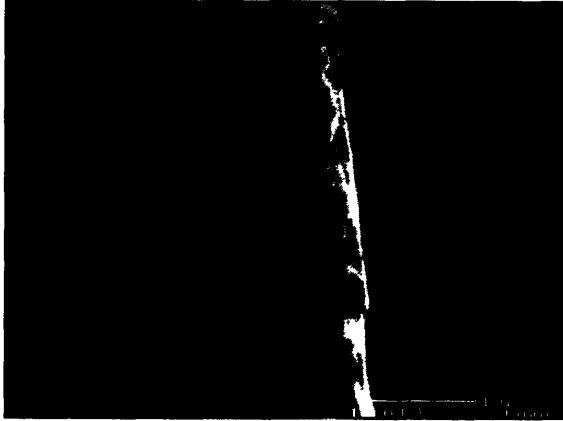
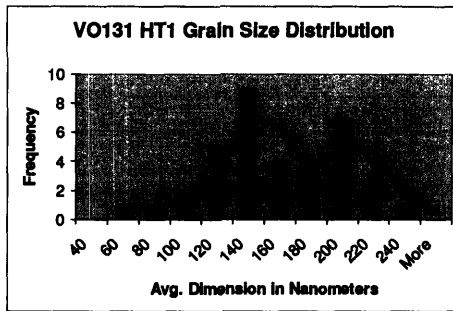
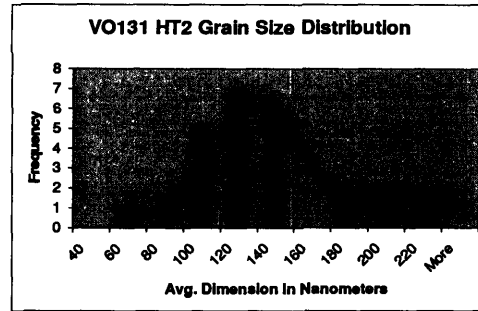


Image 8: VO132 HT4 (Note: 20Kx mag.)

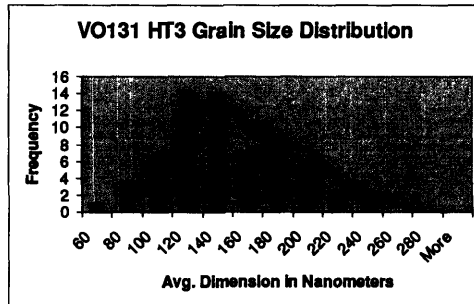
As is discernable in these images, grains of many different sizes are present in each sample. Therefore, simply calculating a single dimension as the average grain size overlooks an important degree of complexity in these thin films. Also, those samples brought to their annealing temperature at a faster ramp rate have a visually distinct appearance from those that were raised to their annealing temperature more slowly (i.e., VO131 HT4 compared to VO132 HT4). To capture the breadth of the grain sizes present in each sample, SEM images were analyzed with the pixel counting feature in Adobe Photoshop. For each grain, a long and short axes of the grain were measured in an effort to capture two dimensions of the grain shape. The number of grains within a certain size grouping was determined by assembling the grains according to the average of their two measured dimensions. The results of these calculations and a line indicating the moving average grain size for each sample is shown in the histograms below (Graphs 3-10).



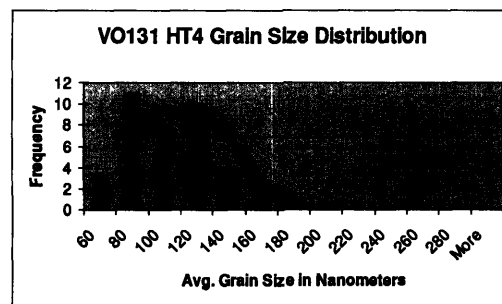
Graph 3



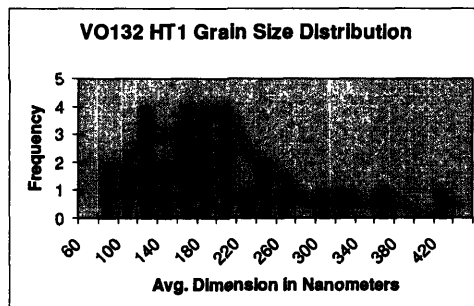
Graph 4



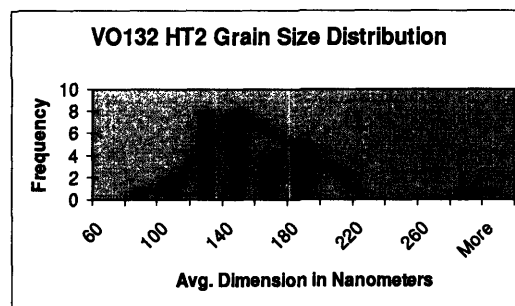
Graph 5



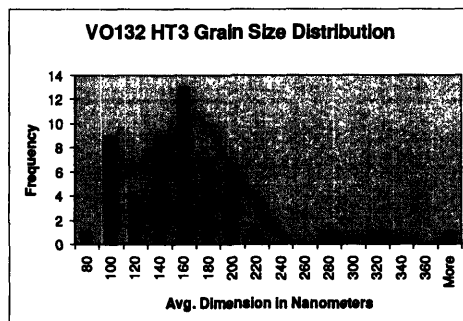
Graph 6



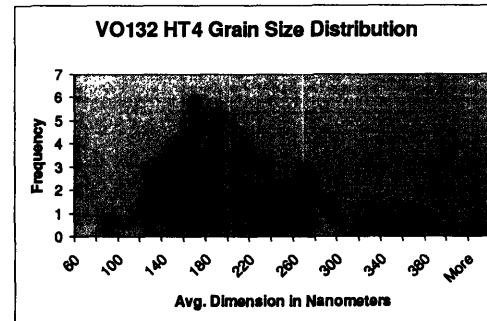
Graph 7



Graph 8



Graph 9



Graph 10

Different samples of similar average grain size show remarkably variant distributions of grain sizes about their average. The average grain sizes, as determined by analysis of SEM images, are shown in Table 3. Samples annealed at the highest temperatures (400 and 500°C) for a short time (90 min), such as VO131 HT4 and VO132 HT2, have the narrowest distributions of grain sizes. Broader grain size distributions were present when the samples were annealed for 24 h at elevated temperature for crystallization. It is suspected that the longer anneal leads to a broader range of grain sizes because coarsening is able to occur among some grains during the increased time at the annealing temperature. During the 90-min holds at 400 and 500°C, many small grains are nucleated quickly; however, there is insufficient time at the high annealing temperature for larger grains to coalesce into their smaller neighbors and grow.

Table 3: Average Grain Sizes as Determined by SEM Analysis

| Sample | Mean Grain Size (nm) | Standard Deviation (nm) |
|---------------|-----------------------------|--------------------------------|
| VO131 HT1 | 144.9 | 42.16 |
| VO131 HT2 | 122.4 | 38.53 |
| VO131 HT3 | 135.3 | 40.43 |
| VO131 HT4 | 91.12 | 22.94 |
| VO132 HT1 | 177.4 | 81.96 |
| VO132 HT2 | 137.6 | 38.57 |
| VO132 HT3 | 149.1 | 53.96 |
| VO132 HT4 | 188.5 | 74.67 |

Also, a weak correlation between the average grain sizes of these samples and the annealing temperature for each sample suggests that a higher annealing temperature leads to a lower average grain size. Samples annealed at higher temperatures had lower average grain sizes regardless of annealing time (note samples VO132 HT1 and VO131 HT4, for examples). At a higher annealing temperature more grains can be nucleated simultaneously and, as a result, the grains cannot grow to as large a size before

impingement occurs. Further growth might be possible in the same sample if it were annealed at a lower temperature for the same time so that fewer crystalline grains were initially nucleated.

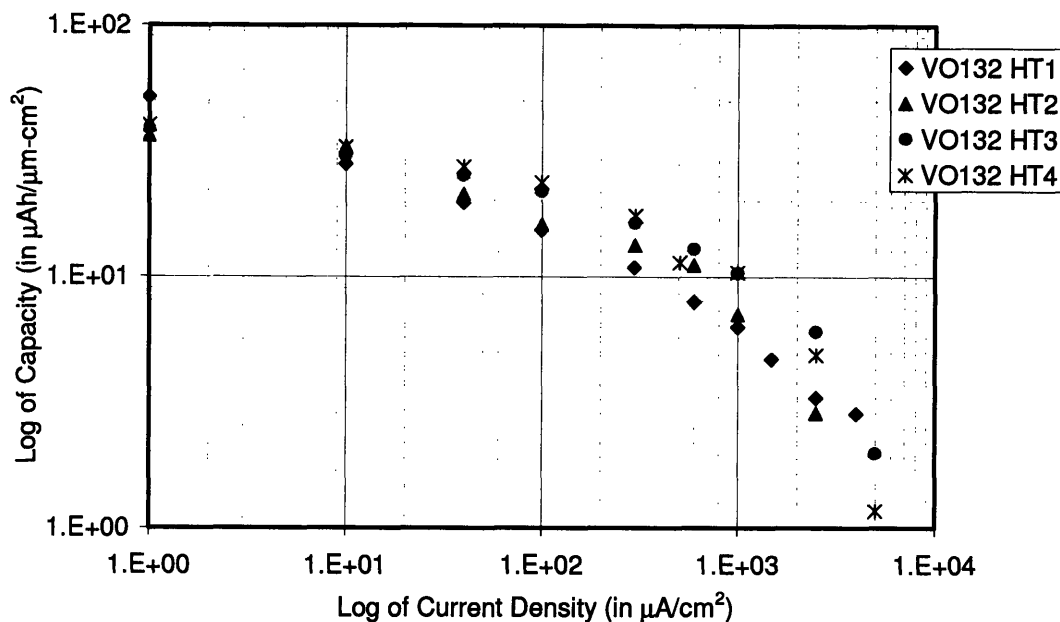
Overall, the differences in average grain size observed in these samples are insufficient for an analysis of differences in behavior between micro- and nano-grains. However, the distribution of grain sizes about each average varies widely from sample to sample, depending on annealing time. As such, the goal of this research will be to determine the electrochemical rate-capability of vanadium oxide thin films with different grain size distributions as cathodes in lithium ion batteries.

IV. ELECTROCHEMICAL ANALYSIS

Capacity-Rate Performance

Following the characterization of each of the vanadium oxide thin films, samples VO132 HT1, VO132 HT2, VO132 HT3, and VO132 HT4 were assembled into coin cells. The vanadium oxide functioned as the working electrode in the liquid electrolyte cell with lithium metal serving as both the counter and reference electrodes. Once the cells were assembled and determined to have a non-zero open circuit voltage, they were connected to a Solartron 1286 Potentiostat for current rate testing. The cells were tested at a range of currents between 1, 10, 40, 100, and 200 $\mu\text{A}/\text{cm}^2$ and were further cycled at higher rates if capacity had not fallen off after the 200 $\mu\text{A}/\text{cm}^2$ cycle (up to 5,000 $\mu\text{A}/\text{cm}^2$). The results of this current rate testing are illustrated on a graph of capacity versus current density on the following page (Graph 11).

VO132 Current Rate Test Results

**Graph 11**

As was noted in the SEM analysis of samples VO132 HT1 and VO132 HT2, VO132 HT1 has a large average grain size (177.44 nm) and a broad distribution of grain sizes about the average. In contrast, VO132 HT2 has a smaller average grain size (137.6 nm) and a narrow distribution of grain sizes about the average. From these current rate tests, it appears that the capacity-rate performance of these cells is comparable to within a statistical margin of error.

The capacity-rate performance patterns found for samples VO132 HT3 and VO132 HT4 were very similar. However, at the highest current rates, VO132 HT4 did exhibit a slightly faster drop off than VO132 HT3. VO132 HT3 has a smaller average grain size (149.1 nm) than VO132 HT4 (188.5 cm) and also a narrower distribution of grain sizes than VO132 HT4.

There does not seem to be a correlation between average grain size and capacity-rate performance; however, there is a minor trend linking rate performance and average grain size distribution width. Those samples with a narrower average grain size distribution demonstrated slightly improved performance (e.g. VO132 HT2 and VO132 HT3). In such samples, most of the grains are approximately the same size, and there will be a grain boundary to grain surface area ratio at the cathode surface which is approximately constant across the cathode. In samples with broader grain size distributions, there may be regions on the cathode surface where there are greater or lesser relative ratios of grain boundaries to bulk crystalline grain. As such, the diffusion of lithium ions in these broad distribution samples may be uneven over the cathodes surface and result in a faster decrease in battery capacity with increasing current rate.

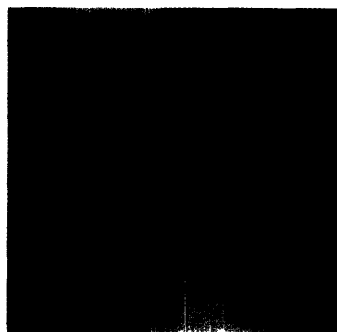
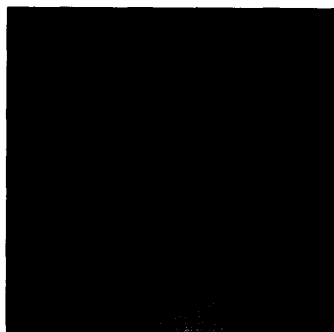
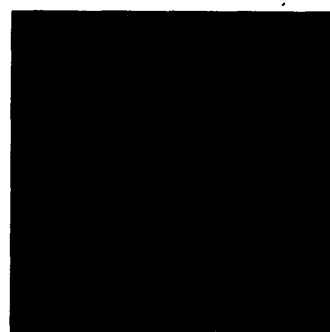
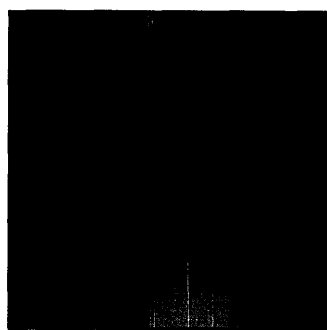
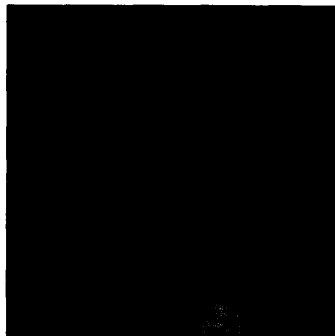
Atomic Force Microscopy (AFM)

To characterize the diffusion of lithium ions through vanadium oxide grains and grain boundaries during the discharging process, in situ AFM observations of a VO132 HT2 coin cell were attempted. A VEECO Scanning Electrochemical Potential Microscope was utilized to capture images of the VO132 HT2 coin cell. An area 250 nm by 250 nm was scanned as the cell discharged. Images were recorded throughout the cell discharging process so that changes in the material surface and grain boundary dimensions, most specifically grain size at the surface, could be recorded.

If changes in the surface grain area and grain boundaries could be measured accurately, one would be able to differentiate the rates at which smaller grains or larger grains are growing under the influence of flowing current. If a difference in the growth rates of a smaller grain and a larger grain in the same sample could be noted, then

differences in capacity-rate performance and diffusion behavior noted between samples with broad versus narrow average grain size distributions may be observed.

Unfortunately, image drift, image quality, and software available for analysis (Nanoscope Image and Nanoscope Control by Digital Instruments) were inadequate in this study to measure small changes in grain size. However, if these issues could be resolved, it is speculated that one would note smaller grains growing at a relatively faster rate than larger grains because they have a greater surrounding grain boundary to bulk grain surface ratio. Images 9-14 show several of the AFM images and the corresponding voltages.

**Image 9 (3.072 V)****Image 10 (3.043 V)****Image 11 (2.997 V)****Image 12 (2.934 V)****Image 13 (2.839 V)****Image 14 (2.740 V)**

Galvanostatic Intermittent Titration Technique (GITT)

GITT measurements were conducted on sample VO132 HT2 to determine the baseline behavior of the chemical diffusion coefficient for lithium ions in a vanadium oxide-lithium liquid electrolyte system. Although GITT was not performed on all the samples considered in this study, the same phase change behavior and general trends in chemical diffusion coefficient may be expected of all the vanadium oxide samples, regardless of their particular heat treatment.

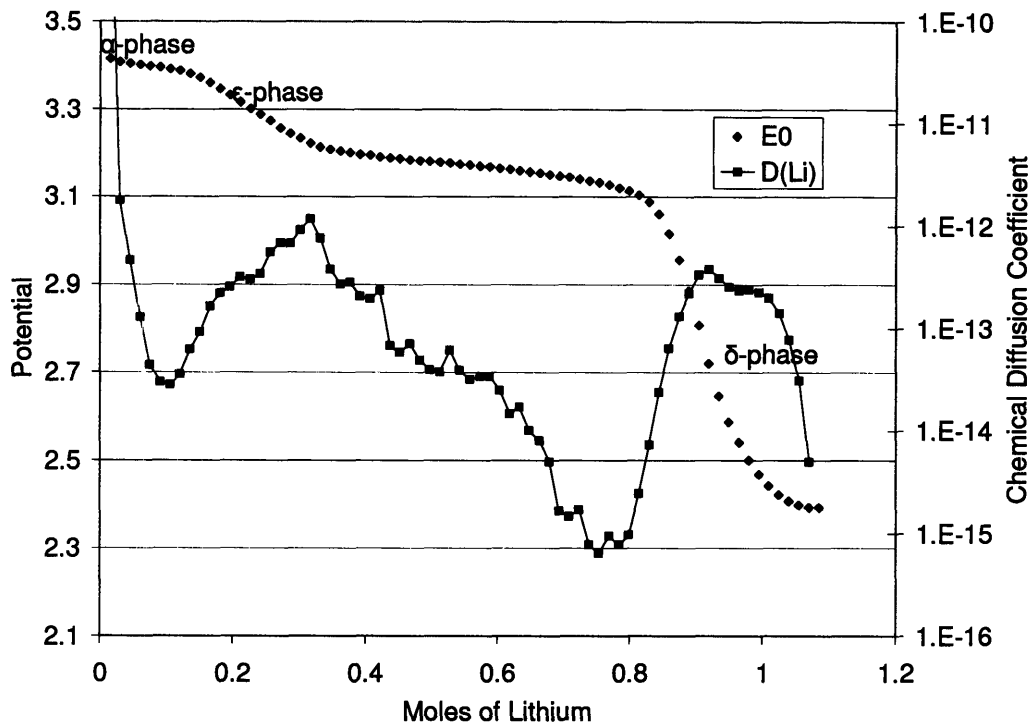
In GITT experiments, a cell with VO132 HT2 cathode material was discharged over time. Estimates of the system's behavior were obtained during the cell discharging process. A fixed current was driven for a set time interval through the cell by a Solartron

1286 Potentiostat. Between current pulses, the system was given time to equilibrate at which time the potential was measured.¹² Using thermodynamic relationships compiled by the work of Weppner and Huggins,¹³ the behavior of the chemical diffusion coefficient and phase changes in the crystalline vanadium oxide material may be tracked with the instant lithium concentration in the cathode material.

As the lithium concentration in the cathode increased during the discharging process, the vanadium oxide cathode material passed through two distinct phase changes. Initially, at very low lithium concentration the stable form of vanadium oxide was observed to be α -phase (α - $\text{Li}_x\text{V}_2\text{O}_5$, where $0 < x < 0.13$). In the region where $0.13 < x < 0.32$, the vanadium oxide is transformed to the ϵ -phase. A second phase change occurred when the lithium molar concentration reached $x = 0.80$ and 0.88 taking the vanadium oxide from its ϵ -phase to δ -phase.

The regions where phases change are illustrated in Graph 12. Two-phase regions are identifiable by their relatively constant potential with change in lithium concentration. This constant potential is indicative of the constant chemical activity for both phases within the two-phase change region. The potential is able to decrease more drastically in the discharging process in the single-phase regions, when chemical activity varies significantly with lithium concentration. In single-phase regions, the vanadium oxide crystal structure is physically rearranging itself by expanding layers so that it may internally accommodate the storage of more lithium¹⁴. Additionally one may note that the chemical diffusion coefficient is greater immediately following a phase change, when there are more empty lithium sites in the vanadium oxide crystal structure, than it is at the upper bound for lithium concentration in that single-phase region. As such, the chemical

diffusion coefficient of lithium into vanadium oxide is dependent on both the lithium concentration and phase of the cathode material.



Graph 12: GITT Results for VO132 HT2

The lithium chemical diffusion coefficient does not vary monotonically with lithium concentration; instead, it appears to fluctuate as increasing amounts of lithium are incorporated into the vanadium oxide crystal structure, as shown in Graph 12. The chemical diffusion coefficient is observed to decrease when the vanadium oxide is present as a single phase and increase in two-phase regions. The diffusion coefficient decreases in single-phase regions as the lithium concentration within that region increases because the available sites for lithium movement are progressively occupied thereby reducing lithium mobility for that phase's crystal structure.

The values for the chemical diffusion coefficient are derived from Fick's Law, which assumes that one is observing a single-phase system. Therefore, the diffusion coefficient for the two-phase regions is undefined¹⁵. The diffusion coefficient in these regions is shown in Graph 12 merely for consistency purposes and does not represent actual system properties.

V. CONCLUSION

Overall, the performance of vanadium oxide thin-film cathodes on ITO-coated glass substrates showed greater dependence on the distribution of grain sizes in a sample than on the average grain size. It has been shown that narrower grain size distributions, as determined through SEM analysis, correlated with better capacity-rate performance than wider grain-size distributions. Future studies to determine the exact diffusion mechanisms causing these differing capacity rates should be conducted with the aid of in situ AFM and in situ XRD measurements.

VI. ACKNOWLEDGEMENTS

The author would like to especially thank Simon Mui for his invaluable guidance and assistance in this research.

The author would also like to thank Professor Donald Sadoway for his advice and sponsorship, Anne Clemencon from Professor Yang Shao-Horn's group for her assistance with AFM experimentation, and the members of the Sadoway Group: Ken Avery, Elsa Olivetti, and Patrick Trapa.

REFERENCES

-
- ¹ Levi, M.D., Z. Lu, and D. Aubach. "Li-insertion into thin monolithic V₂O₅ films electrodes characterized by a variety of electroanalytical techniques." *Journal of Power Sources*. 97-98 (2001): 482-485.
- ² Weppner, W. and R.A. Huggins. "Determination of the Kinetic Parameters of Mixed-Conducting Electrodes and Application to the System Li₃Sb." *Journal of the Electrochemical Society*. 124 (10, October 1977): 1569-1578.
- ³ Chiu, K.-F., F.C. Hsu, G.S. Chen, and M.K. Wu. "Texture and Microstructure Development of RF Sputter-Deposited Polycrystalline Lithium Transition Metal Oxide Thin Films." *Journal of the Electrochemical Society*. 150 (4, 2003): A503-A507
- ⁴ Ramana, C.V., R.J. Smith, O.M. Hussain, and C.M. Julien. "On the growth mechanism of pulsed-laser deposited vanadium oxide thin films." *Materials Science & Engineering B*. 111 (2004): 223.
- ⁵ Antolini, Ermete. "LiCoO₂: formation, structure, lithium and oxygen nonstoichiometry, electrochemical behaviour and transport properties." *Solid State Ionics*. 170 (2004): 159-171.
- ⁶ Levi, et al.
- ⁷ Satto, Christine, Philippe Sciau, Eric Dooryhee, Jean Galy, and Patrice Millet. "The δ- >ε ->γ 'High Temperature' Phase Transitions Evidenced by Synchrotron X-Ray Powder Diffraction Analysis." *Journal of Solid State Chemistry*. 146 (1999): 103-109.
- ⁸ Galy, Jean, Christine Satto, Philippe Sciau, and Patrice Millet. "Atomic Modeling of the δ <-> ε LiV₂O₅ Phase Transition and Simulation of the XRD Powder Pattern Evolution." *Journal of Solid State Chemistry*. 146 (1999): 129-136.
- ⁹ Murphy, D.W., P.A. Christian, F.J. DiSalvo, and J.V. Waszczak. "Lithium Incorporation by Vanadium Pentoxide." *Inorganic Chemistry*. 18 (1979): 2800-2803.
- ¹⁰ Galy, et al.
- ¹¹ Ibid.
- ¹² Weppner, W. and R.A. Huggins.
- ¹³ Ibid.
- ¹⁴ Galy, et al.
- ¹⁵ Mui, S.C., A.M. Mayes, and D.R. Sadoway. "Microstructure Effects on the Electrochemical Kinetics of Vanadium Pentoxide Thin Films." Unpublished manuscript.